This is a repository copy of *Identification of flutter derivatives from full-scale ambient vibration measurements of the Clifton Suspension Bridge*.

White Rose Research Online URL for this paper:
http://eprints.whiterose.ac.uk/99222/

Version: Accepted Version

Article:

Identification of flutter derivatives from full-scale ambient vibration measurements of the Clifton Suspension Bridge

Nikolaos Nikitas[1]*, John H. G. Macdonald[1] and Jasna B. Jakobsen[2]

[1]Department of Civil Engineering
University of Bristol, University Walk, Bristol, BS8 1TR, UK
[2]Department of Mechanical and Structural Engineering and Material Science
University of Stavanger, N-4036, Stavanger, Norway

Abstract. The estimated response of large-scale engineering structures to severe wind loads is prone to modelling uncertainties that can only ultimately be assessed by full-scale testing. To this end ambient vibration data from full-scale monitoring of the historic Clifton Suspension Bridge has been analysed using a combination of a frequency domain system identification method and a more elaborate stochastic identification technique. There is evidence of incipient coupling action between the first vertical and torsional modes in strong winds, providing unique full-scale data and making this an interesting case study. Flutter derivative estimation, which has rarely previously been attempted on full-scale data, was performed to provide deeper insight into the bridge aerodynamic behaviour, identifying trends towards flutter at higher wind speeds. It is shown that, as for other early suspension bridges with bluff cross-sections, single-degree-of-freedom flutter could potentially occur at wind speeds somewhat below requirements for modern designs. The analysis also demonstrates the viability of system identification techniques for extracting valuable results from full-scale data.

---

* Corresponding author, E-mail: N.Nikitas@bristol.ac.uk

1 INTRODUCTION

For full-scale structures the most rational way to proceed with predictions of the reliability and operational safety includes identification methods from response only measurements. Especially for existing bridges, treatment of the flutter instability can substantially be verified in this way. No analytical solutions exist for the fluid forces on the bluff bridge cross-sections to identify the critical wind speed, so inevitably each investigation has to adopt some experimental or semi-empirical foundation to proceed to a further assessment. Most commonly wind tunnel tests of scale models are used for reproducing the flutter phenomenon leaving the question of the effects of scaling issues. Even minor details such as deck railings or roadway grills and vents can strongly alter aerodynamic performance (see Jones et al. 1995 and Matsumoto et al. 2001). Hence, only analysis of the response of the real bridge can clarify the validity of wind tunnel tests and even reveal aspects, which either due to modelling assumptions or to loading irregularities, were previously concealed.

Aeroelastic parameters have rarely been obtained from full-scale bridge data. Jakobsen and Larose (1999) addressed the problem on the Höga Kusten Bridge and presented a comparative analysis with wind tunnel results using a subspace identification technique for extraction of flutter derivatives. Costa and Borri (2007) essentially applied the same identification routine (Jakobsen 1995, Jakobsen & Larose 1999), both on numerically simulated responses and on measured data from the Iroise Bridge, finding good performance of the method in each case. For both of these bridge studies, the identification routine itself was found to be reliable when tested using simulated data (including with added noise) or against other methods for wind tunnel data. Comparisons between full-scale and wind tunnel results were not unreasonable, but since the full-scale bridges were far from flutter, the trends in the flutter derivatives were not very clear.

2

Another approach to the problem of identifying the aerodynamic effects on full-scale bridge vibration characteristics, but without quantifying flutter derivatives, was used by Macdonald (2003) on the Second Severn Crossing. Variations of effective damping ratios and natural frequencies with wind speed were found and some indications of aeroelastic modal coupling were identified on the partially constructed bridge (Macdonald & Daniell 2005). In other full-scale studies, Littler (1992) and Brownjohn (1994) on the Humber Bridge, Bietry et al. (1994) on the Saint-Nazaire Bridge, Ge and Tanaka (2002) on the Höga Kusten Bridge during construction and Jensen et al. (1999) on the Great Belt Bridge, Nagayama et al. on the Hakucho Bridge all found some trends of effective aerodynamic damping with wind speed, but coupling between modes and flutter derivatives were not identified.

The limited number of full-scale studies from which aeroelastic parameters have been found makes any new cases useful for furthering knowledge of the viability of such system identification from site data and for interpreting actual bridge behaviour.

2   THE CASE STUDY

In the current paper, analysis is performed on full-scale vibration measurements from the historic Clifton Suspension Bridge (CSB), shown in Fig. 1. The CSB spans the Avon Gorge in Bristol, UK and was designed by I.K. Brunel in 1830, although it was not completed until 1864 (Barlow 1867). It was one of the longest suspension bridges of that time, with a main span of 214m. Wrought iron chains provide the suspension system, being the common practice for such early long-span bridges. In the light of modern understanding of bridge aerodynamics, the bridge cross-section (Fig. 2) and its light weight make it potentially susceptible to wind-induced vibrations. Indeed, on a few occasions in its lifespan large amplitude vibrations in strong winds have been reported.

On Christmas Day 1990 there was evidence of vertical motion at the bridge ends of the order of 250mm, which translates to even larger amplitudes within the bridge span. Both verti-

cal and torsional deck motions were evident on a video recording of the bridge towards the end of the storm. A similar large vibration event was reported on 3 December 2006. Although no wind recordings exist from the bridge site itself on these occasions, data from the nearest weather stations imply that the maximum 1-hour mean wind speeds could have been around 20m/s. For recordings on site with wind speeds up to 16m/s, coupling action between the first vertical and torsional modes seemed to occur (Section 3.2) and the maximum vertical displacement of the end of the bridge was 35mm (and the maximum measured elsewhere 92mm). The coupling action between modes and the rapid growth of vibration amplitudes for a modest increase in wind speed indicate strong aeroelastic effects, making the bridge behaviour rather interesting. Such characteristics are reminiscent of features observed, in a more severe form, on the Tacoma Narrows (Farquharson et al. 1950-1954) and Deer Isle (Kumarasena et al. 1989a,b) bridges.

It is worth noting that ten suspension bridges from the same era as the CSB failed due to wind between 1818 and 1889, including the Menai Straits Bridge and a span of the Brighton Chain Pier (Farquharson et al. 1950-1954). In contrast the CSB has survived virtually unscathed for over 140 years. According to empirical estimates, as in most bridge design rules, it is potentially susceptible to flutter with an estimated critical wind speed of only around 20m/s. Therefore adverse aeroelastic effects could become significant in moderately strong winds.

For the current study, the wind conditions and bridge response recordings over two winter periods, from November 2003 to March 2004 and from December 2007 to February 2008, are used. The data include several occasions with moderately strong winds, and reasonable ranges of wind speeds and directions, thus enabling a meaningful assessment of the wind effects on the bridge dynamics.

Two ultrasonic anemometers were mounted 61m either side of midspan, more than 5m above road level. Nine accelerometers were positioned at a series of cross-sections along the

bridge during an earlier analysis of the CSB dynamic response, enabling mode shapes to be identified (Macdonald 2008). For the records considered here, two sets of three accelerometers were positioned at midspan and at a cross-section slightly off centre (26.8m from midspan) as illustrated in Fig. 1. This location was chosen as the reference cross-section since all significant vibration modes could be measured there. Signals from all instruments were passed through anti-aliasing filters with a cut-off frequency of 4Hz and were recorded at a sampling rate of 12.5Hz. The primary aim of this study was to uncover details of large amplitude response that the bridge was found to produce for certain wind conditions by determining the variation of modal characteristics with wind velocity and explore the possibility for flutter instability.
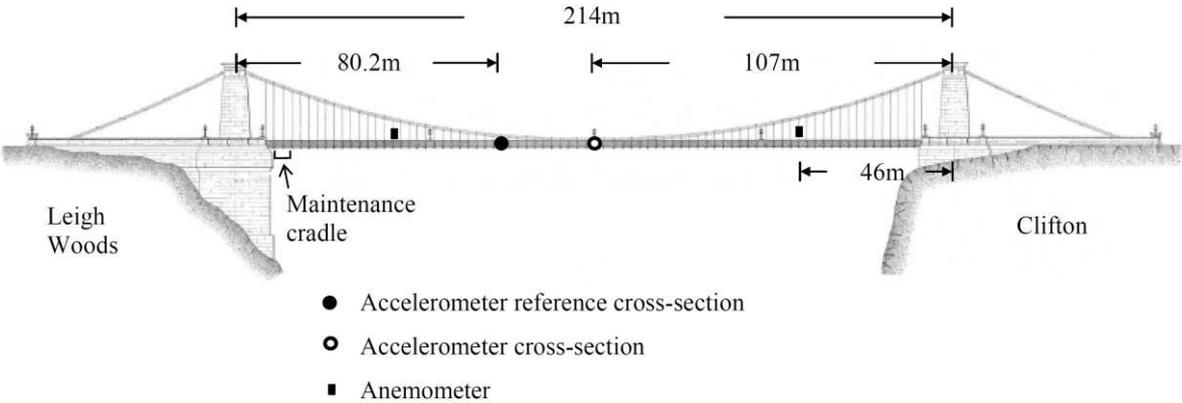
Fig. 1 Bridge elevation showing instrument locations. Based on figure after Barlow (1867), with permission from Thomas Telford Publishing.

Modal parameter estimates from a frequency based curve fitting technique (for details see Macdonald and Daniell 2005) are used here, together with a subspace stochastic identification formulation especially modified to extract flutter derivatives (Jakobsen 1995). In this study, due to lack of wind tunnel data from a scale model, flutter derivatives of other typical bridge cross-sections, as presented by Scanlan and Tomko (1971), are used to assess potential similarities. Cross-sections employed for comparative purposes are chosen to represent both the low structural depth and the high parapets (perforated on the CSB), of the section in hand.

5

The paper consists first of a short discussion on the acquired wind measurements. Typical wind speeds and wind turbulence conditions are described and the local terrain effects are discussed. Subsequently attention is moved to the bridge response details. A conventional modal analysis is performed based on linear modelling and all modal characteristics are identified. The last part containing the flutter derivative identification scheme first presents the employed Covariance Block Hankel Matrix (CBHM) formulation and subsequently discusses the flutter potential of the CSB case study.
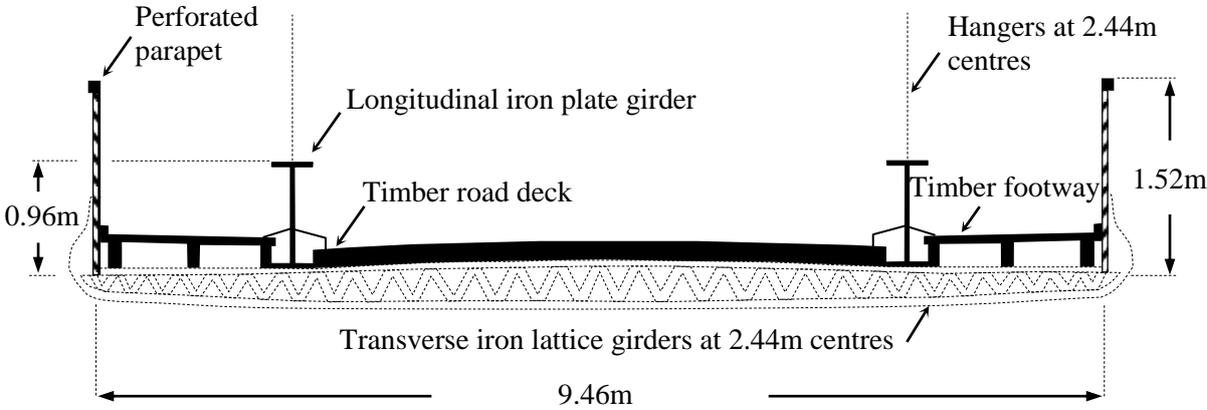
Fig. 2 Sketch of the bridge cross-section.

3　WIND CHARACTERISTICS

The topography around the CSB has a considerable effect on the local wind characteristics. As shown in the polar plots from both anemometers in Fig. 3, the wind speeds follow certain trends with orientations. (True North is at 31˚ relative to the axes shown). The trends differ markedly from the general wind pattern in the region away from the local effects. The strongest winds in the absence of topographic effects are typically from the south-west direction (at about 250˚ on these axes). The stronger winds, as measured, are aligned along the gorge and can be easily explained by funnelling of the flow in these orientations and sheltering due to the high ground near the bridge ends. Strong winds from the south-west are greatly attenuated at the bridge site, and virtually no wind from the north-east quadrant is experienced at the site. It was also observed that the correlation of the wind directions and wind speeds measured by

the two anemometers was strongly influenced by the wind orientation. In particular, for wind directions close to along the gorge the phenomenon was rather pronounced with even a small change in wind direction resulting a large variation in the ratio between the two individual anemometer wind speed values.

The maximum wind speed, averaged over one hour (unless stated all wind information hereafter refer to 1-hour means), did not exceed 16m/s at the bridge site, although higher speeds were measured at the nearest weather stations, for winds from the south-west. A histogram of 1-hour average wind speeds at the bridge is given in Fig. 3. Maximum 1 second gusts were of the order of 26m/s for both anemometers.
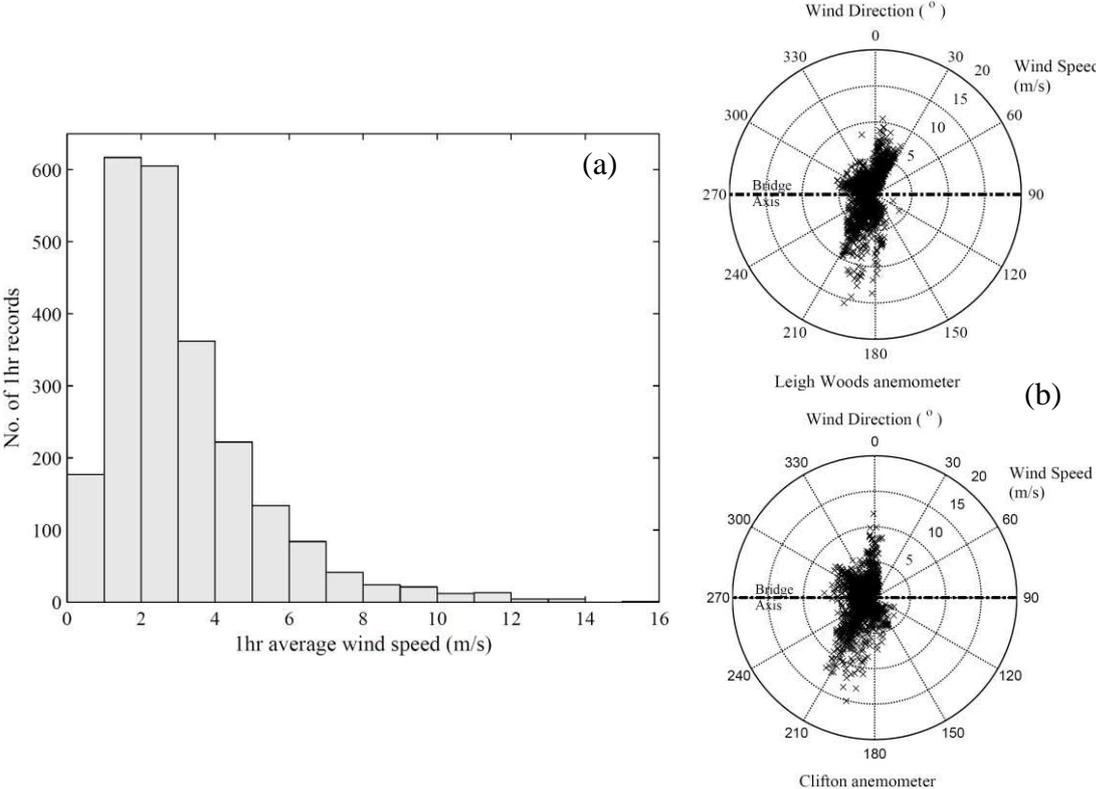
Fig. 3 (a) Histogram of wind speeds during the 2003-04 recording period. (b) Polar plots of 1-hour mean wind velocities from both anemometers.

In addition, the wind turbulence and angle of attack parameters were considered. For wind turbulence there was a strong dependence on wind direction and a weaker one on wind speed. High levels of turbulence (up to 60% longitudinal turbulence intensity) were experienced, par-

ticularly for wind not along the gorge and for lower wind speeds. In winds over 8m/s, which only occurred along the gorge, approximately normal to the bridge, the mean longitudinal turbulence intensity was 21% and the mean vertical turbulence intensity 10%. The vertical and across-wind turbulence intensities followed very similar patterns to the longitudinal turbulence. For longitudinal turbulence intensities up to 40%, the across-wind turbulence was approximately equal to it and the vertical turbulence intensity approximately half of the value. These are typical of relationships between the three components of turbulence. For higher turbulence intensities measured, generally in lower wind speeds, the vertical and across-wind turbulence intensities were relatively larger.

For the vertical angle of attack there was also strong dependence on the wind direction, and there were noticeable differences in the measurements from the two anemometers. The presence of the bridge itself is likely to have affected these measurements, as well as the topography of the gorge, since the anemometers were relatively close to the deck. High vertical angles of attack occurred, up to approximately $\pm10°$. (It should be noted that these values are all averaged over 1 hour periods). There was no significant difference in vertical angles of attack for different wind speeds.

A final wind aspect significant for the subsequent analysis refers to the frequency content of wind buffeting. Although the traffic loading seems to be reasonably well captured by a white noise loading approximation (predominantly from step loading as vehicles drive onto or off the suspended span), the same does not hold for wind. By comparing spectral estimates deduced for various combinations of wind and traffic loading it was found that above approximately 0.25Hz the wind loading spectra appeared as 1/f noise with a power exponent -8/3, thus producing a general loading spectrum approximated by a relation of the form:

$$S_{load}(f) = S_w\, f^{-8/3} + S_t,\tag{1}$$

where: S_w is a constant for a given record, being a function of the wind parameters,

f is frequency and

S_t is the magnitude of white noise traffic loading for the particular record.

The frequency power exponent of -8/3 is as expected for the 'high frequency' tail of the wind buffeting load spectrum, for a 3D aerodynamic admittance function inversely proportional to frequency.

4   RESPONSE AND MODAL PARAMETERS

4.1   Response Characteristics

Fig. 4 shows the 1-hour average wind speeds over the whole of the first monitoring period, and the corresponding Root Mean Square (RMS) vertical accelerations at the reference cross-section. The RMS amplitudes normally show a clear daily cycle with the varying traffic load, with a maximum vertical response of approximately $0.02m/s^2$. By comparison it can be seen that only in wind speeds exceeding approximately 8m/s does the response noticeably exceed the maximum traffic-induced response. The maximum wind-induced acceleration measured was approximately four times the maximum traffic-induced acceleration. The torsional and lateral acceleration responses at the reference cross-section followed very similar patterns to the vertical response over the monitoring period, although the magnitudes of the responses were lower. The maximum instantaneous value of each component was found to be approximately six times the 1-hour RMS value.

Dynamic displacements were calculated from the measured accelerations by double integration and it was noticed that the response is dominated by low frequency modes. The dominance of the low frequency modes is caused by the relatively higher wind loading at low frequencies and the effect of the integration, which exaggerates low frequency components. Whereas the maximum RMS acceleration due to wind loading was approximately four times

9

the maximum due to traffic loading, in terms of displacement the maximum RMS response to wind was approximately 10 times that for traffic.
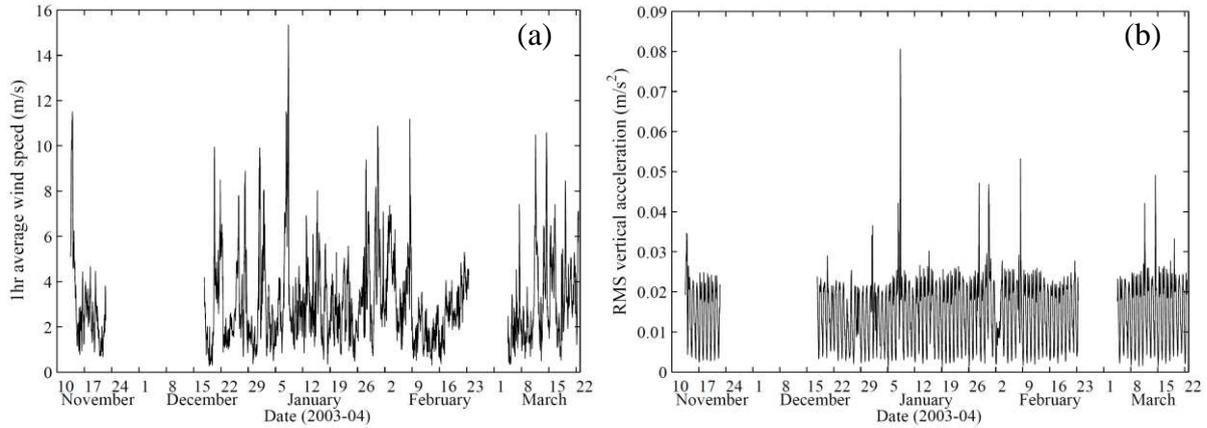
Fig. 4 (a) 1hr average wind speed over the monitoring period. (b) 1-hour RMS vertical accelerations at the reference location over the monitoring period.
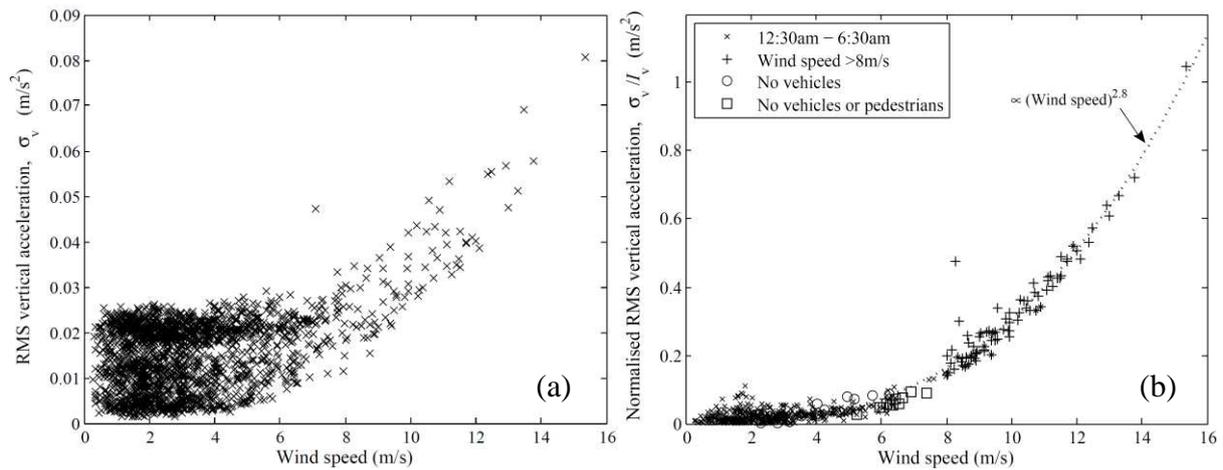
Fig. 5 (a) RMS vertical accelerations in relation to wind speed for all 1hr records. (b) Same as (a) for 1hr records dominated by wind loading. Now in y-axis RMS vertical accelerations are divided with the relevant vertical turbulence intensity. The power-law approximating the obtained trend is also plotted.

The influence of wind loading on the measured vertical accelerations is shown in Fig. 5. Similar figures were obtained for the lateral and torsional accelerations. The scatter of results, particularly at low wind speeds, is largely due to the varying traffic contribution. The varying wind turbulence intensity also had an effect. Excluding records dominated by traffic and normalising by the corresponding wind turbulence intensity gives a much clearer relationship with wind speed as shown on the right of Fig. 5. RMS responses are then close to power law functions of the wind speed with a power exponent of approximately 3.

4.2 Modal Analysis

Modal parameters were calculated from the acceleration Power Spectral Densities (PSDs) using the Iterative Windowed Curve-fitting Method (Macdonald and Daniell 2005), specifically developed for the analysis of ambient vibration data and allowing for the previously specified loading spectrum. The method iteratively curve fits in the frequency domain a series of windowed (performing the same window function the measured spectra employ) idealized Single-Degree-of-Freedom transfer functions, taking into account both the loading spectra and the multi-modal interplay. Measurements were only taken on the suspended bridge deck, but all modes inevitably involve vibrations of other parts of the structure, particularly the chains. Analysis was performed for frequencies up to 3Hz with twelve vertical, eleven torsional and four lateral modes being identified in this range, based on measurements in low wind speeds (Macdonald 2008). Typical PSDs for three different loading scenarios for vertical, torsional and lateral accelerations are given in Fig. 6 to present the effect of wind loading on the bridge response. An important finding is the proximity of the first vertical and torsional modes, with natural frequencies of 0.293Hz and 0.356Hz respectively (ratio 0.82). These are the first anti-symmetric modes of each type and it appears that in the stronger winds they start to couple in a potentially incipient flutter motion as evidenced by the small hump at 0.35Hz in the vertical spectrum, as seen in Fig. 6(a) and more clearly in Fig. 7.

In Fig. 7 (left) the responses for the highest 1-hour wind speed (15.3m/s) were filtered below 0.47Hz and modified, by subtracting the responses in the next higher (symmetric) modes from midspan measurements, to only include motion of the first two modes. The peak in the vertical PSD at the torsional frequency is strong evidence of coupling action. The coupling was not evident for low winds and became stronger for higher winds (Fig. 7 right), showing it to be an aeroelastic effect. The coherence between the vertical and torsional accelerations showed similar evidence, with the value around 0.35Hz rising to approximately 0.6 in high

11

winds compared with typical values below 0.4 in low winds and at other frequencies. It is also worth noting that the next pair of modes showed a similar tendency for coupling action in strong winds, due to their similar shapes (first symmetric mode of each type) and close natural frequencies (ratio $0.424/0.498 \approx 0.85$). The next section discusses in more detail the identification of the CSB flutter derivatives, so as to be able to quantify the observed coupling signs and the potential for flutter.
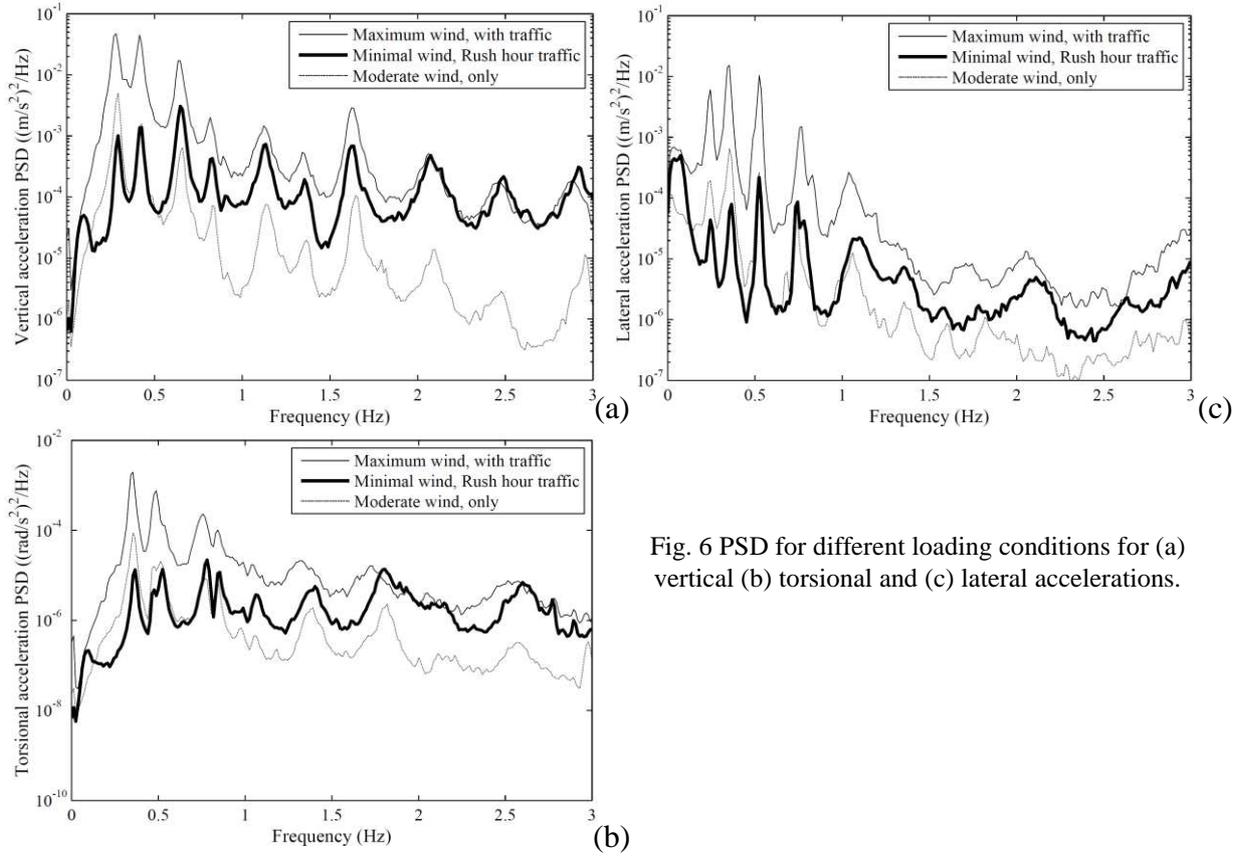
Fig. 6 PSD for different loading conditions for (a) vertical (b) torsional and (c) lateral accelerations.

5 FLUTTER DERIVATIVES

5.1 Flutter Analysis

According to the semi-empirical Selberg (1963) equation for bridge sections resembling flat plates, an estimate for the flutter speed is given by:

$$\frac{U_F}{f_{\theta 0} B} = C \sqrt{\frac{r_g m}{\rho B^3} [1 - (\frac{f_{z0}}{f_{\theta 0}})^2]} \quad , \tag{2}$$

where U_F is the flutter speed, B the deck width, r_g the radius of gyration, m the total mass per unit length, C a constant depending on the mode shape similarity and the section's behavioural resemblance to flat plate, ρ the air density and f_{z0} and $f_{\theta0}$ the still air vertical and torsional natural frequencies. For the first pair of natural frequencies, described above, and for $\rho = 1.2$kg/m^3, B = 9.46m, C = 2 and the approximate values m = 5370kg/m, r_g = 4m, the flutter onset speed is estimated as 18m/s, or 14m/s using the more conservative variant of Eq. (2) in the British design rules (British Standards Institution 2009). These are very low values. This is due to the low torsional natural frequency, the close neighbourhood of vertical and torsional modes, their shape affinity and the low mass per unit length. However, the bridge cross-section is not a flat plate and the uncertainty in the value of C means Eq. (2) is not very reliable, but it gives a first approximation for the flutter speed that is within the range of wind speeds potentially occurring at the site.

For evaluating the flutter behaviour the classical 2D formulation of Scanlan and Tomko (1971) is adopted, where aeroelastic forces are taken as a linear combination of the modal displacements and velocities appropriately multiplied with the so-called flutter derivatives. The motion-dependent lift and pitching moment L_{ae} and M_{ae} are hence given by

$$L_{ae} = \frac{1}{2}\rho U^2 B\left[kH_1^*\frac{\dot{z}}{U} + kH_2^*\frac{B\dot{\theta}}{U} + k^2 H_3^*\theta + k^2 H_4^*\frac{z}{B} \right] \;, \tag{3}$$

$$M_{ae} = \frac{1}{2}\rho U^2 B^2\left[kA_1^*\frac{\dot{z}}{U} + kA_2^*\frac{B\dot{\theta}}{U} + k^2 A_3^*\theta + k^2 A_4^*\frac{z}{B} \right] \;. \tag{4}$$

where U is wind speed, z vertical displacement, θ rotation and $k=\omega B/U=2\pi/U_r$ is reduced frequency, which is proportional to the number of oscillation cycles during the free stream flow passage over the width B.

In this 2D formulation, the motion-induced drag force, D_{ae}, and the effects of the along-wind motion are ignored. Under the assumption of low damping, as generally implied in the model-

ling of self-excited forces and conventional bridge flutter analysis, the flutter derivatives H_i^* and A_i^* with i=1,2,3,4 become only functions of the reduced frequency k (or equivalently of the reduced wind speed U_r), Chen (2007).

5.2   Identification Method

A state space formulation of the dynamic problem can be assembled using the Covariance Block Hankel Matrix Method (CBHM method), which is founded on the widespread Eigen-value Realization Algorithm (ERA) described by Juang and Pappa (1985). The formulation in ERA is identical to CBHM with the exception that instead of the Markov parameters containg Impulse Response Functions (IRFs), covariance estimates of output measured random data are employed. Jakobsen (1995) first applied CHBM in the estimation of flutter derivatives from wind tunnel tests and later on, the method found extensive application on aerodynamic applications and testing. Qin and Gu (2004), Mishra et al. (2006), Siringoringo and Fujino (2008) all thoroughly describe the matrix derivation. Brownjohn et al. (2010) found a relative advantage of the method toward other operational modal analysis approaches. Synoptically it should be referred that the method is based on the Singular Value Decomposition (SVD) and appropriate factorization of a Hankel matrix built up by covariance estimates of the output (i.e. displacements in this application) time series. If y stands for the displacement matrix with z and θ in rows in this case, then the unbiased sample cross covariance matrix to be used in the Hankel matrix construction is given by

$$C_{yy}(i+n,i) = C_{yy}(n) = \frac{1}{N-n}\sum y(i+n)y^T(i), \qquad n = 0,1,..,l. \qquad (5)$$

where n is the number of sampling intervals for the discrete time delay nΔt, N is the number of samples in the time series, l is the maximum number of lags considered and i is a counting index. The biased estimate, which only differs in the use of the denominator N instead of N – n, can be used instead with negligible differences for long time records. The method typically

assumes white noise loading but here it was attempted to also account for the actual loading spectra shape. Thus ordinary filtering in frequency domain was used on the response data to account for the previously presented in Eq.(1) coloured lift and moment spectra. The main attribute that has to be taken care of is preserving after filtering the exact coupling between modes, that was artificially altered during filtering. The filter has the monotony of the loading spectra (declining) so in the current case it is expected that the side effect of reduced coupling will be introduced. This is not realistic because buffeting action for each mode is uncorrelated to the coupling action due to self-excited forcing between modes. The remedy for this inconsistency was to finally modify coupled induced flutter derivatives with the ratio of the filter values so as to recover the initial coupling. Additional information on the performance of identifications with coloured noise and specific attributes on the relative sensitivity of each derivative are described by Jakobsen (1995) For the specific problem in hand the effect of the actual wind load on flutter derivatives was found to be insignificant.

The decomposition of the Hankel matrix recovers all parameters of the discrete time realisation. Knowing the modal stiffness and damping matrices for the in-wind and still air cases (pure structural stiffness and damping contributions) allow one to separate the flutter derivatives. The whole method (having the dimensionality for the problem already described as trivially 2 degrees-of-freedom) relies on the choice of two parameters; the length of the individual time record N and the number of time delays l for which the covariance matrix is evaluated and stored in the block Hankel matrix. The choice of both is investigated through a sensitivity analysis together with inspection of the time evolution of the auto and cross-covariance functions.

5.3 Application to the CSB

The proximity of the fundamental vertical and torsional modes, as presented in Fig. 7, seems to encourage some coupling action, which could potentially be the initial signs of clas-

sical flutter. The PSDs in Fig. 7 imply some non-negligible values of H_2^* or H_3^* flutter derivatives since a coupling contribution is evidently occurring in the vertical PSD at the torsional frequency. The flutter derivative identification was performed in one case with recorded acceleration data and in another with double integrated displacements evaluated from the accelerations in hand. Both cases produced identical results.
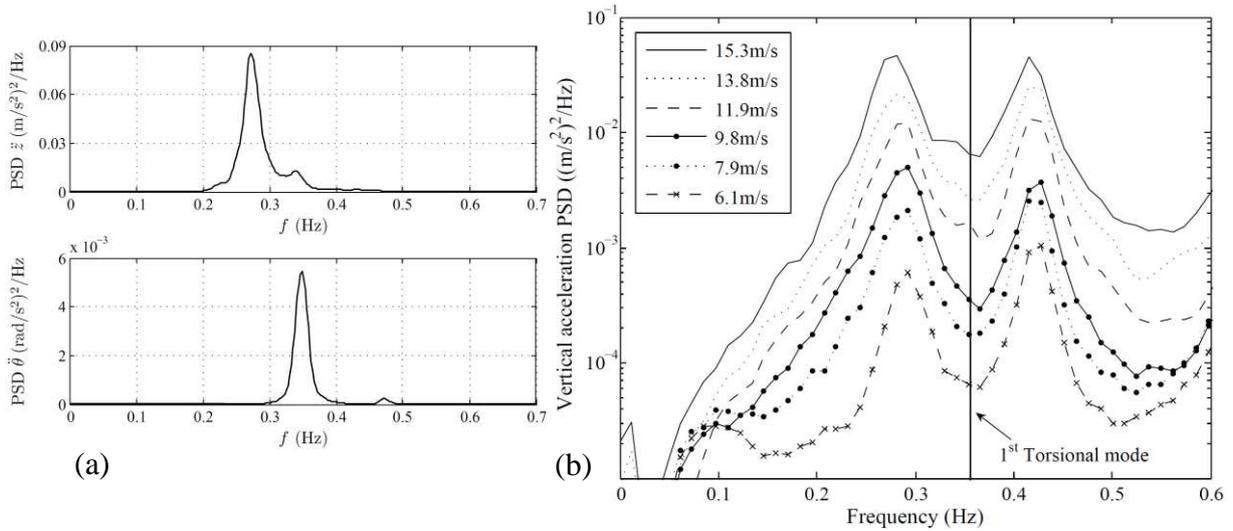
Fig. 7 (a) PSDs of filtered data for first vertical and torsional modes for the maximum wind speed record. (b) The evolution of the coupling action is evident in the vertical PSD for wind speeds above 11m/s.

For selection of the two foresaid identification parameters a range for time records from 10 minutes to 1 hour and, for the covariance function length, lags in the range of 10 to 40 seconds were used, preserving analogies with similar previous treatments. Example covariance functions, for moderately strong wind, are plotted against time in Fig. 8. As previously demonstrated by Jakobsen et al. (2003), the suitable number of maximum time lags is strongly influenced by the response character at different wind speeds. Higher wind speeds usually allow only a shorter meaningful portion of the covariance function for accurately reproducing the 2 degree-of-freedom interaction, e.g. due to high aerodynamic damping of the pure vertical response in case of streamlined box-girders. For our case an optimum set of values was found to be the combination of 15 minute records (N = 11 x 2^{10}) with time delays up to 20

16

seconds (l = 250) with only weak sensitivity to l, probably due to the relatively small range of wind speeds.
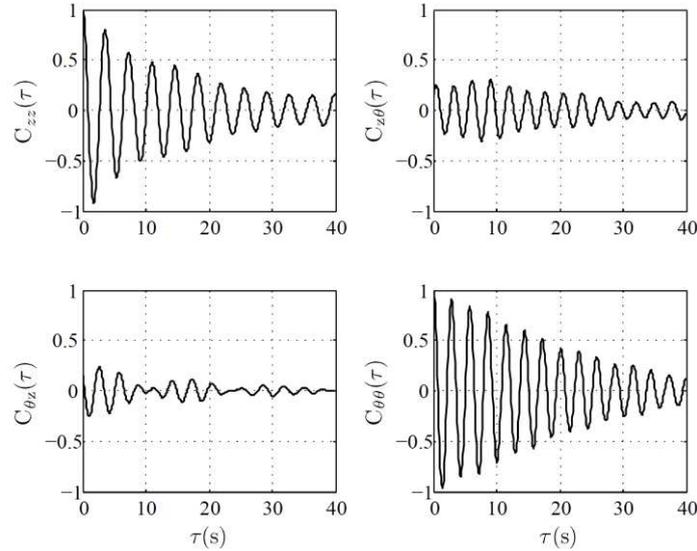
Fig. 8 Covariance functions for the combined two degrees-of-freedom plotted against time.

Results for the CSB flutter derivatives are given in Fig. 9. No wind tunnel tests have been undertaken on the CSB deck section, but where possible the site data are compared with available wind tunnel results of other deck cross-sections. Sign conventions for aerodynamic forces are as in Scanlan and Tomko (1971), i.e. with the lift force and the vertical displacement pointing downwards and the overturning moment and the rotation positive for the windward side of the bridge girder moving upwards. A sensitivity analysis on the measured wind characteristics, such as the turbulence and the angle of attack, proved not to be able to reproduce a clear picture of their effect. The identified trends of flutter derivatives remained unaltered, but data were insufficient to quantify a systematic impact of the investigated parameters.
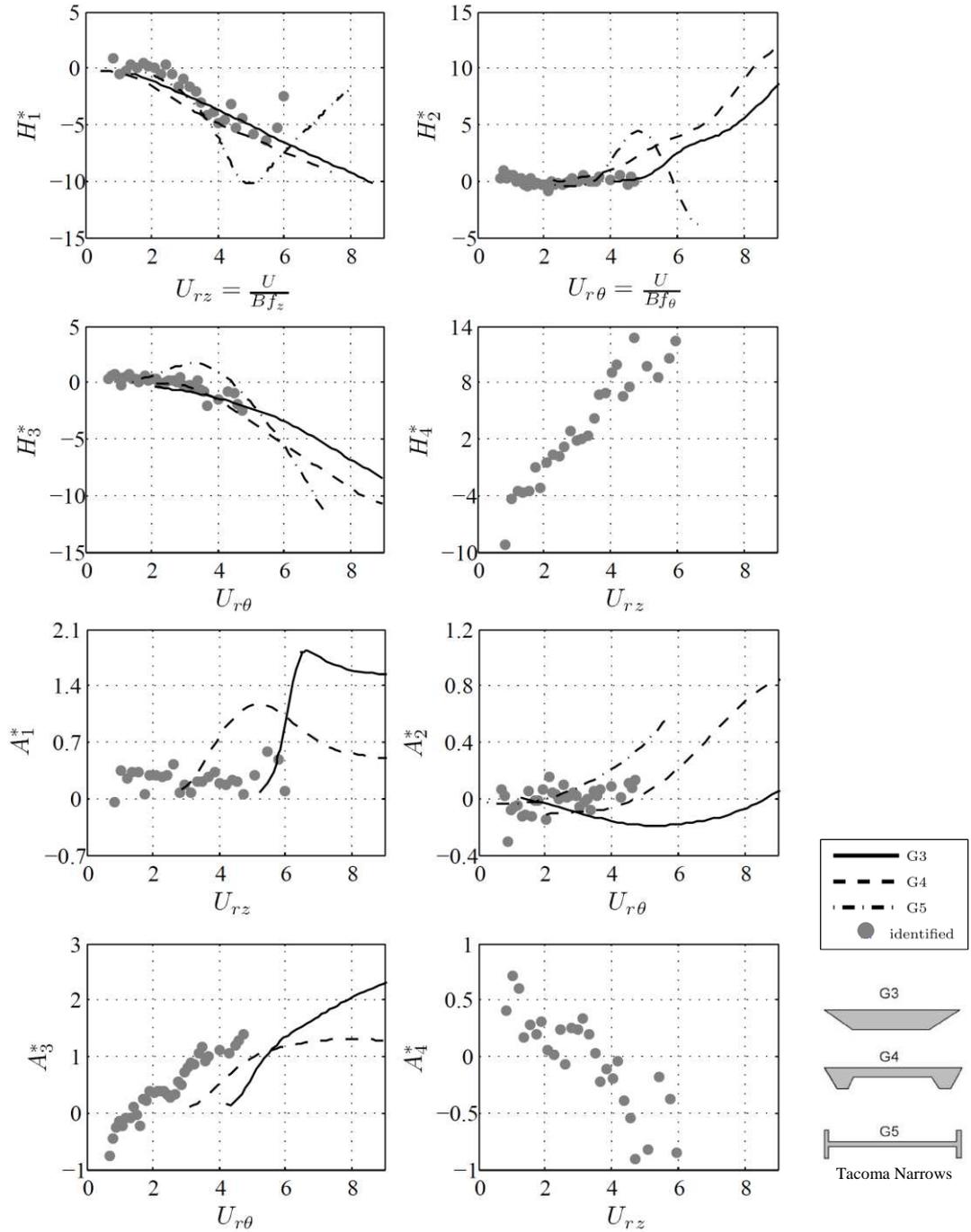
Fig. 9 Flutter derivatives of Clifton Suspension Bridge from full scale data, compared with wind tunnel extracted flutter derivatives for various cross-sections (after Scanlan and Tomko 1971 and adapted to Eqs. (3) and (4)). A_1^* and A_3^* for section G5 are negligible. H_4^* and A_4^* were not measured in the wind tunnel tests. Identified values correspond to binned and averaged identified values.

Some of the derivatives in Fig. 9 appear to have an offset for still-air wind conditions. This has also been encountered in previous treatises (Jakobsen 1995), and here can mostly be attributed to effects such as the distortion from traffic effects, including both loading and variation in the mass distribution, as well as uncertainties in the modal masses and inaccuracies in

18

the still-air structural matrices. For off-diagonal still-air values there is no remedy for this off-set, which can be attributed to record noise and imperfections as explained by Hoen (2006). For diagonal values there was an attempt to minimize the offset for damping derivatives, since their absolute values are of greater importance.

Although the identified flutter derivatives are noisy, unsurprisingly for full-scale ambient data, some trends are apparent. Consistent with the observed bridge behaviour, the results indicate that, within the range of wind speeds recorded (maximum 15.3m/s), the bridge is not susceptible to pure vertical or torsional flutter (so called "damping-driven flutter" as presented by Matsumoto et al. 1996), which was the reason for the famous Tacoma Narrows Bridge collapse. This is due to having close to negative H_1^* and A_2^* (direct damping derivatives), which will probably need a further increase in reduced wind speed to initiate such alarming behaviour, if indeed it does occur. However, H_1^* apparently shows a steep positive gradient near the highest wind speed recorded, suggesting it could become positive for higher wind speeds, possibly leading to flutter. This trend persists regardless of the selected identification parameters (N and l), indicating it is not due to numerical errors, although the last few points in the figure are from averages over few records, so their accuracy may be limited. Fig. 10 shows the H_1^* flutter derivative estimates from each 15-minute record, before the averaging used for Fig. 9. Although only the last few points show the apparent positive gradient, these points depart significantly from the trend at lower reduced velocities and the differences are greater than the general scatter of points, implying there is a real effect. If this is confirmed, the effect of possible positive H_1^* (i.e. negative damping) could provide a feasible explanation for the occasional observations of large vibrations of the bridge in strong winds.
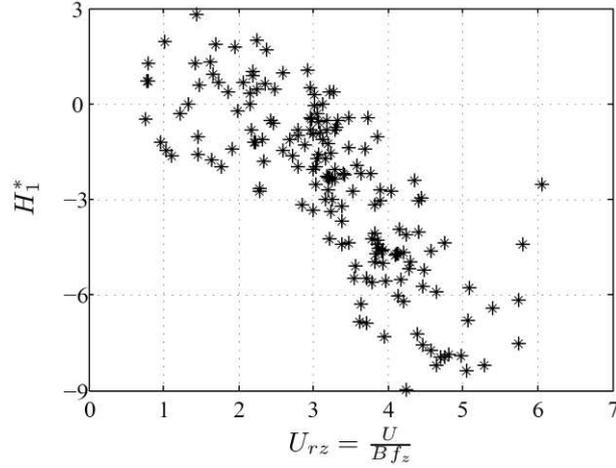
Fig. 10 H_1^* flutter derivative from each 15-minute record

Dimensionally assessing the possibility of unstable motion in the vertical response, a value of $H_1^* \approx 6$ needs to be reached. This estimate is based on the low amplitude structural damping ratio of $\zeta = 3.3\%$ for the vertical mode (Macdonald 2008) and on the assumption that no beneficial amplitude-dependent increase in structural damping takes place. The structural damping is believed to be so high compared with modern suspension bridges because of the many joints in the structure, particularly the wrought iron suspension chains. Particular care had been taken in the system identification method to avoid bias errors that can often lead to erroneous overestimation of damping (Macdonald & Daniell 2005).

The H_2^* and H_3^* derivatives, which control the coupling from torsional to vertical motion, have small values. However at the higher wind speeds there is a noticeable growing negative trend in H_3^*, in line with the curves for other bridge profiles, which potentially explains the previously illustrated coupled spectra in Fig. 7. The relative influence of H_3^* for the evidently coupled response record translates to a vertical force approximately 1/10 of the peak restoring elastic force for the mode.

The evolution of H_4^* reflects the reduction of vertical natural frequency with increasing wind speed, although this could alternatively be due to an amplitude dependence rather than the wind. Similarly A_3^* illustrates the reduction in the torsional natural frequency. The shape

20

of A_3^* (with a high positive gradient in comparison to other bridge cross sections) may at first sight raise concern for the possibility of static divergence, but actually this is quite far off since the estimated required value of A_3^* for such a case is 12.6. Similarly for H_4^* the critical value is found to be 76. Such values reinforce previous observations that, unlike airfoil flutter, for bridges with bluff sections aeroelasticity influences more the damping than the frequencies of the modes (see Scanlan and Tomko 1971 and Billah and Scanlan 1990), although in this case coupling was also apparent.

In any case, from the sections in hand a qualitative similarity was found with the bluff section of Tacoma Narrows. For a proper estimation of the critical flutter wind speed, through Complex Eigen-Value analysis (CEV), data inclusive of higher wind speeds are needed to extend the plots of Fig. 9.

According to Matsumoto et al. (1996) there is a mutual dependence between flutter derivatives, based on the fact that twisting θ and the apparent angle of attack associated with the bridge girder vertical velocity generate similar motion depended forces. The following relations were proposed:

$$H_1^* = kH_3^* \quad , H_4^* = -kH_2^* \quad , A_1^* = kA_3^* \quad , A_4^* = -kA_2^*. \tag{6}$$

These relations were found to yield an accurate match for many bluff cross sections. Thus taking into account the slight similarity to the Tacoma Narrows section which suffered a pure torsional failure due to A_2^*, Eq. (6) can be employed to investigate the possible extension of A_2^* through the knowledge of A_4^*. This can be achieved since the scaling of the reduced wind speed for A_4^* uses the lower vertical frequency giving higher reduced wind speeds than A_2^*, which is expressed in relation to the torsional frequency. Consequently it is possible to review the possibility of a single degree-of-freedom torsional flutter on the CSB. Fig. 11 shows the A_2^* data with the resulting additional points. Fitting the polynomial $A_2^* = 0.12U_{r\theta}(0.3U_{r\theta} - 1)$ provides an estimate for pure torsional flutter at $U_{r\theta} \approx 6.3$ i.e. at $U \approx 21$m/s. This estimate is

based on the low amplitude structural damping estimate for the torsional mode of $\zeta = 2.6\%$ (Macdonald 2008) and does not allow for a potential beneficial increase of structural damping with amplitude. Both because of this and the uncertainty in the estimation of such small aerodynamic forces as presented by A_4^*, the actual flutter wind speed could be higher, although results of this magnitude are still significantly below today's standards.
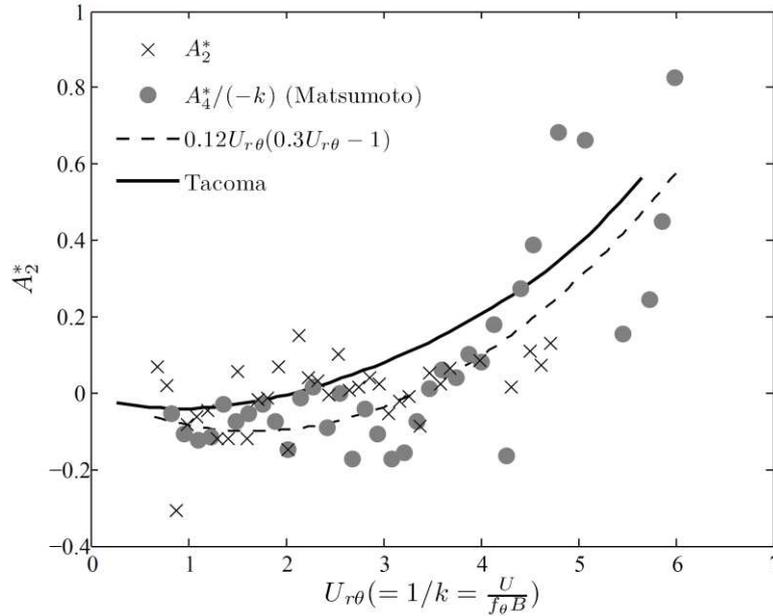
Fig. 11 Flutter derivative A_2^* with additional points from A_4^* as suggested by Matsumoto et al. (1996). The fitted polynomial, indicated by broken line, was used for estimation of a pure torsional flutter wind speed.

6 CONCLUSIONS

The measured full-scale wind-induced response of the Clifton Suspension Bridge has been analysed and flutter derivatives extracted using a subspace stochastic identification method. Trends in flutter derivatives have been identified and were found to have some similar features to the Tacoma Narrows Bridge. For the historic Clifton Suspension Bridge, which has been in service for more than 140 years to date, the results indicated no problem within the range of wind speeds recorded (up to 15.3m/s) although there were potential concerning trends in the flutter derivatives for higher wind speeds. Operation at wind speeds so close to potential instabilities provided unique full-scale data of a bridge in this condition, making it an interesting case study. Aeroelastic coupling was identified between the close first vertical

22

and torsional modes. However, the actual potential hazard appears to be from single-degree-of-freedom instabilities, with the potential for negative aerodynamic damping caused by positive H_1^* or A_2^*. As a matter of fact for first time ever there was a flutter wind speed estimation based solely on the actual full-scale dynamic performance of a bridge.

This paper attempts to contribute to the literature on the analysis of aeroelastic effects from ambient vibration data on full-scale bridges, being one of very few similar studies. It shows the viability of extracting flutter derivatives from full-scale data and the potential value of system identification methods to validate full-scale performance of structures.

AKNOWLEDGEMENTS

REFERENCES

Barlow, W.H. (1867), "Description of the Clifton Suspension Bridge", Minutes Proc. ICE, **26**, 243-257, (reprinted Proc. ICE: Bridge Engineering, **156** (BE1), 5-10, 2003).

Bietry, J., Delaunay, D. and Conti, E. (1995), "Comparison of full-scale measurements and computation of wind effects on a cable-stayed bridge", J. Wind Eng. Ind. Aerodyn., **57**, 225-235.

Billah, K.Y. and Scanlan, R.H. (1990), "Resonance, Tacoma Narrows bridge failure, and undergraduate physics textbooks", Am. J. Phys., **59**, 118-124.

British Standards Institution (2009), "Published Document: Background information to the National Annex to BS EN 1991-1-4 and additional guidance", BS PD 6688-1-4:2009.

Brownjohn, J.M.W. (1994), "Estimation of damping in suspension bridges", Proc. ICE: Structures and Buildings, **104**, 401-415.

Brownjohna J.M.W., Magalhaes F., Caetano E. and Cunha A. (2010), "Ambient vibration re-testing and operational modal analysis of the Humber Bridge", Eng. Struct., **32**, 2003–2018.

Chen, X. (2007), "Improved understanding of bimodal coupled bridge flutter based on closed-form solutions", ASCE J. Structural Engineering, **133** (1), 22-31.

Costa, C. and Borri, C. (2007), "Full-scale identification of aeroelastic parameters of bridges", 12th Int. Conf. Wind Engineering, Cairns, Australia, 799-806.

Farquharson, F.B., Smith, F.C. and Vincent, G.S. (1950-1954), Aerodynamic stability of suspension bridges with special reference to the Tacoma Narrows Bridge (five parts), Engineering Experiment Station, University of Washington, USA

Ge Y.J. and Tanaka, H. (2002), "Aerodynamics of long-span bridges under erection", J. Struct. Engrg., 126, 1404-1412.

Hoen, C. (2006) "Subspace identification of modal coordinate time series", 24th International Modal Analysis Conference, IMAC XXIV, St.Louis, USA.

Jakobsen J.B. and Hjorth-Hansen E. (1995), "Determination of the aerodynamic derivatives by a system identification method", J. Wind Eng. Ind. Aerod., **57**, 295-305.

Jakobsen, J.B. and Larose, G.L. (1999), "Estimation of aerodynamic derivatives from ambient vibration data", 10th Int. Conf. Wind Engineering, 837-844.

Jakobsen, J.B., Savage, M.G. and Larose, G.L. (2003), "Aerodynamic derivatives from the buffeting response of a flat plate model with stabilizing winglets", 11th Int. Conf. Wind Engineering, Lubbock, Texas, 673-680.

Jensen, J.L., Larsen, A., Andersen, J.E. and Vejrum, T. (1999), "Estimation of structural damping of Great Belt suspension bridge", Pr*oc. 4th Euro. Conf. Struct. Dyn. (Eurodyn '99)*, Prague, 801-806.

Jones, N.P., Scanlan, R.H., Sarkar, P.P., and Singh, L. (1995), "The effect of section model details on aeroelastic parameters", J. Wind Eng. Ind. Aerod., **54-55**, 45-53.

Juang J.N. and Pappa R.S (1985), "An eigensystem realization algorithm for modal parameter identification and model reduction", J. Guid. Control Dynam., **8** (5) 620–627.

Kumarasena, T., Scanlan, R.H. and Morris G.R. (1989), "Deer Isle: Efficacy of stiffening system", Journal of Structural Engineering, **115**, No 9, 2297-2312.

Kumarasena, T., Scanlan, R.H. and Morris G.R. (1989), "Deer Isle: Field and computed vibrations", Journal of Structural Engineering, **115**, No 9, 2313-2328.

Littler, J.D. (1992), "Ambient vibration tests on long span suspension bridges", J. Wind Eng. Ind. Aerodyn., **42**, 1359-1370.

Macdonald, J.H.G. (2003), "Evaluation of buffeting predictions of a cable-stayed bridge from full-scale measurements", J. Wind Eng. Ind. Aerodyn., **91**, 1465-1483.

Macdonald, J.H.G. and Daniell, W.E. (2005), "Variation of modal parameters of a cable-stayed bridge identified from ambient vibration measurements and FE modelling", Engineering Structures, **27**, 1916-1930.

Macdonald, J.H.G. (2008), "Pedestrian-induced vibrations of the Clifton Suspension Bridge, UK", Proc. ICE: Bridge Engineering, **161** (BE2), 69-77.

Matsumoto, M., Koboyashi, Y. and Shirato, H. (1996), "The influence of aerodynamic derivatives on flutter", J. Wind Eng. Ind. Aerodyn., **60**, 227-239.

Matsumoto, M., Nakajima, N., Taniwaki, Y. and Shijo, R. (2001), "Grating effect on flutter instability", J. Wind Eng. Ind. Aerod., **89**, 1487-1498.

Mishra S.S, Kumar K. and Krishna P. (2006), "Identification of 18 flutter derivatives by covariance driven stochastic subspace method", Wind Struct., **9** (2), 159-178.

Nagayama T., Abe M., Fujino Y., Asce M. and Ikeda K. (2005), "Structural Identification of a Nonproportionally Damped System and Its Application to a Full-Scale Suspension Bridge", J. Struct. Eng. (ASCE), **131**, 1536-1545.

Qin X.R and Gu M. (2004), "Determination of flutter derivatives by stochastic subspace identification technique", Wind Struct., **7** (3), 173-186.

Scanlan, R.H. and Tomko, J.J. (1971), "Airfoil and bridge flutter derivatives", J. Eng. Mech. Div., ASCE, **97** (EM6), 1717-1737.

Selberg, A. (1963), "Aerodynamic effects on suspension bridges", Int. Conf. Wind Effects on Buildings and Structures, Vol. II, 462-479.

Siringoringo D.M and Fujino Y. (2008) , "System identification of suspension bridge from ambient vibration response", Eng. Struct., **30**, 462–477.